

1                   A Fast Detection Method for Wheat Mould Based on Biophotons

2

3   Short title: Fast Detection for Wheat Mould by Biophotons

4

5   Gong Yue-hong<sup>1</sup>, Yang Tie-jun<sup>1</sup>, Liang Yi-tao<sup>1</sup>, Ge Hong-yi<sup>1,2</sup>, Chen Liang<sup>3</sup>

6

7   <sup>1</sup> School of Information Science and Engineering, Henan University of Technology, Zhengzhou,

8   China

9   <sup>2</sup> Key Laboratory of Grain Information Processing & Control, Ministry of Education, Henan

10   University of Technology, Zhengzhou, China

11   <sup>3</sup> College of Biological Engineering, Henan University of Technology, Zhengzhou, China

12

13   \* Corresponding author

14   E-mail: [tjyanghlyu@126.com](mailto:tjyanghlyu@126.com)

16

## 17 **Abstract**

18           Mould is a common phenomenon in stored wheat. First, mould will decrease the quality  
19 of wheat kernels. Second, the mycotoxins metabolized by mycetes are very harmful for humans.  
20 Therefore, the fast and accurate examination of wheat mould is vitally important to evaluating its  
21 storage quality and subsequent processing safety. Existing methods for examining wheat mould  
22 mainly rely on chemical methods, which always involve complex and long pretreatment  
23 processes, and the auxiliary chemical materials used in these methods may pollute our  
24 environment. To improve the determination of wheat mould, this paper proposed a type of green  
25 and nondestructive determination method based on biophotons. The specific implementation  
26 process is as follows: first, the ultra-weak luminescence between healthy and mouldy wheat  
27 samples are measured repeatedly by a biophotonic analyser, and then, the approximate entropy  
28 and multiscale approximate entropy are separately introduced as the main classification features.  
29 Finally, the classification performances have been tested using the support vector  
30 machine(SVM). The ROC curve of the newly established classification model shows that the  
31 highest recognition rate can reach 93.6%, which shows that our proposed classification model is  
32 feasible and promising for detecting wheat mould.

33

34

35

36

37

38

## 39 Introduction

40 Wheat, as a type of global grain, is one of the staple foods that human beings and animals  
41 rely on throughout the world. The history of wheat cultivation can be traced back to ten thousand  
42 years ago, and it has become the second most cultivated crop in the world due to its high  
43 productivity and strong adaptability [1]. As the world population has increased over the last  
44 decade, the consumption of wheat has also increased [2], which can be seen in Fig. 1.

### 45 **Fig. 1. Global Consumption of Wheat and Year-on-Year Percentage from 2009 to 2018.**

46 When a suitable surrounding moisture and temperature is achieved, microorganisms  
47 make great contributions to the wheat mould phenomenon, thus affecting the quality and quantity  
48 of stored wheat [3]. Since mould is inevitable during the wheat storage period, the health of  
49 human beings will be extremely threatened once certain edible food that is made using mouldy  
50 wheat as raw materials are available in their daily lives [4]. Many mycotoxins are metabolized by  
51 mouldy wheat, among which aflatoxin B1 (AFB1) is the most striking contaminant and has the  
52 strongest carcinogenicity [5]. Nearly one quarter of crops in the world are contaminated by  
53 aflatoxins before or during their storage period according to the Food and Agriculture  
54 Organization (FAO). Once feeds and foods are made of mouldy kernels, the AFB1 carried within  
55 will cause a series of illnesses, such as retarded growth, immune suppression, human or animal  
56 death, and so on [6]. Therefore, the development of fast and green techniques for detecting AFB1  
57 in stored wheat kernels is very necessary to ensure human and animal safety.

58 The study of biological photons can be traced to 1923 when the Russian biologist  
59 Gurwitsch used biological detectors to test the roots of onions and found a special phenomenon:  
60 onion cells can produce faint light that can stimulate other cells to accelerate their cell division  
61 [7]. The Italian scientist Coli placed some plant buds on detectors with photomultiplier tubes for

62 measurement and observed an ultra-weak light emission phenomenon [8]. In the later 1970s, led  
63 by West German physicians, biophoton research conducted many experiments and made striking  
64 progress [9]. In the 1980s, biophoton technology was applied to spontaneously detect various  
65 plant seeds, including wheat, celery, soybean, and others, and obtained fruitful achievements.  
66 Subsequently, the scientific team represented by Veselova analysed in detail the quality and  
67 performance of various crop seeds (soybean, barley, sunflower, etc.) using the delayed radiation  
68 of biophotons and found that there is a negative correlation between seed vigour and a delayed  
69 luminescence signal [10]. In recent decades, the research of biophoton technology has made  
70 tremendous development. A large number of experiments have proved that biophoton radiation  
71 is a common life phenomenon that is related to biological and physiological activities, the  
72 generation and synthetization of DNA, and other information exchange or energy transmission  
73 processes. The higher the level of an organism is, the greater intensity of the photon radiation  
74 that is emitted. The research applying of biophoton technology has been mainly conducted in  
75 medical fields, such as medical information diagnosis [11], cancer classification [12], analysis of  
76 brain activities [13], and others. In the cereal storage field, however, biophoton studies mainly  
77 focus on insect intrusion rather than on wheat mould. Duan et al. [14] have applied the  
78 permutation entropy algorithm to analyse the biophoton signals of wheat kernels and then use a  
79 BP network to test the experimental effects. Their proposed algorithm not only improves the  
80 detection rate by 10% but also saves the sample training time [14]. Regarding the detection  
81 process of insect intrusion, spontaneous biophoton emission, which is also known as ultra-weak  
82 luminescence (UWL), has been proven to be a sensitive index at reflecting the mould among  
83 wheat kernels. The main achievements in this paper are that we have measured the UWL of  
84 healthy and mouldy wheat kernels separately using biophotonic technology, calculated the

85 approximate entropy and multiscale approximate entropy as the main classification parameters,  
86 and then, we used the SVM to test the classification performance of newly established model.

87

## 88 **Materials and methods**

89

### 90 **Materials**

91

#### 92 **Wheat kernel samples**

93 The experimental wheat kernels were offered by the Yuda grain barn, Zhumadian city,  
94 Henan Province in 2019. Some pretreatment, such as finding foreign materials and imperfect or  
95 damaged kernels, washing the kernels several times using distilled water, drying the samples to a  
96 certain degree of moisture using special equipment and so on, is very necessary. Subsequently,  
97 the wheat sample is divided into two parts: one is the healthy samples, and the other part is sent  
98 to the College of Biological Engineering to cultivate the mould in the sample with 50%  
99 *Aspergillus flavus*. Regarding the healthy wheat samples, we prepared 240 subsamples weighing  
100  $20.00 \pm 0.01$  g. We use 120 subsamples as the training group (experimental group), and the  
101 remaining 120 subsamples form the testing group. Regarding the mouldy wheat samples, 120  
102 subsamples are used as the training group, and the other 120 subsamples are used as the testing  
103 group. Meanwhile, protective measures should be taken during this process due to the strong  
104 poisonous of AFB1.

105

#### 106 **Equipment**

107 The BPCL-2-ZL, manufactured by Beijing Jianxin Lituo Technology Co., Ltd., was used  
108 to measure the biophotons of healthy and mouldy wheat samples.

109 Fig. 2 shows the whole analysis system, which consists of three parts: ① a detection  
110 chamber, where the tested samples are input; ② a biophoton analyser, mainly including the  
111 photon counting and optical hi-voltage converter device; and ③ computer equipment, which  
112 displays results from the corresponding software on a monitor. The calculated average  
113 background noise of the instrument is 28 counts per second, The high voltage for the test is set as  
114 1030 V, and the testing temperature is  $25.0\pm 0.5^{\circ}\text{C}$ .

115 **Fig. 2. Instrumentation Used in the Experiment.**

116

## 117 **Methods**

118 The whole detection process consists of two parts. One part is selecting the right  
119 environmental parameters. Since the experimental result may be influenced by surrounding  
120 factors, all the experiments should be conducted under the same conditions to minimize the  
121 environmental influences, including the same environmental temperature ( $20\pm 1^{\circ}\text{C}$ ), humidity  
122 ( $25\pm 6\%$ ), and measuring time (8:00 am~18:30 pm). The other part is choosing suitable  
123 experimental parameters. Before testing, each sample was placed for 30 min in a dark space to  
124 decrease the interference from ambient parasitic light. Since the spontaneous biophotonic  
125 radiation of wheat kernels is not strong enough, the sampling interval is set to 10 s in order to  
126 collect ample numbers of biophotons. To better reflect the properties of the UWL signals of the  
127 two types of wheat samples, the total sampling time is extended over 15,000 s. Then, the UWL  
128 signals of the healthy and mouldy wheat kernel samples are measured separately.

## 129 **Results**

130

### 131 **Biophotonic data analysis**

132 One hundred and twenty groups of healthy and mouldy wheat samples were measured by  
133 the above processes. Owing to the nonlinear and random characteristics of the number of  
134 biophotons, we calculated the average numbers of photons for all the samples for both types, and  
135 the results are shown in Fig. 3. Table 1 shows their statistical characteristics, such as the mean,  
136 variance and standard deviation. As Table 1 shows, the statistical biophotonic characteristics of  
137 mouldy wheat are larger than those of healthy wheat. This difference occurs because the  
138 *Aspergillus* fungi that colonized the wheat kernels have much stronger metabolism and  
139 respiration. The large number of biophotons in mouldy wheat also provides a convincing  
140 explanation, which coincides with physiological regularity such that the higher the level of an  
141 organism is, the greater the intensity of the biophotons it emits.

142 **Fig. 3. Average UWL Data of Healthy and Mouldy Wheat.**

143 **Table 1. UWL Data Statistical Characteristics of Two Types of Wheat.**

	Mouldy wheat kernels in 2019	Healthy wheat kernels in 2019
Mean	84.22	71.11
Variance	5830.37	3533.45
Standard deviation	76.36	59.44

144 To effectively distinguish between healthy wheat and mouldy wheat based on UWL data,  
145 we will use the approximate entropy (ApEn) and multiscale approximate entropy (MApEn)  
146 algorithm, and then comparing their performances.

147

## 148 **Approximate entropy**

149 The approximate entropy (ApEn) algorithm was proposed by the scholar Pincus to  
150 measure the characteristics of random series [15]. The more complex an initial time series is, the  
151 larger its corresponding ApEn. The ApEn is suitable for analysing the biophoton signals of  
152 wheat kernels because of its more robust performance. Two prominent advantages of the ApEn  
153 are its lower dependency on the length of the initial time series and strong resistance to the noise  
154 contained in the original data.

155 The complete computing process of the ApEn is [16]:

156 Divide the original series  $X = \{x(i), i = 1, 2, \dots, N\}$  into an  $m$ -dimensional vector  $u(i)$ ,  
157 which is shown as follows:

$$158 \quad u(i) = \{x(i), x(i+1), \dots, x(i+m-1)\}, i = 1, 2, \dots, N-m+1 \quad (1)$$

159 Here,  $m$  represents the dimension of the pattern vector, and  $N$  denotes the initial length  
160 of the time series.

161 1) Calculate the distance  $d[u(i), u(j)]$  between vector  $u(i)$  and vector  $u(j)$  using formula 2.

$$162 \quad d[u(i), u(j)] = \max_{k=0,1,\dots,m-1} |x(i+k) - x(j+k)| \quad (2)$$

163 2) Count the numbers of  $d[u(i), u(j)] < r$ , where  $r$ , which is known as the similar tolerance  
164 threshold value, is a positive real number. Then, calculate the proportion between

165  $d[u(i), u(j)] < r$  and the total number of vectors, which is labelled as  $C_i^m(r)$  in equation 3.

$$166 \quad C_i^m(r) = (\text{number of } d[u(i), u(j)] < r) / (N - m + 1) \quad (3)$$

167 1) Calculate the logarithm of  $C_i^m(r)$ , and then, obtain its mean using equation 4. Here, the  
168 mean is labelled as  $H^m(r)$ .

169 
$$H^m(r) = \frac{1}{N-m+1} \sum_{i=1}^{N-m+1} \ln C_i^m(r) \quad (4)$$

170 2) By increasing the dimension from  $m$  to  $m+1$  and repeating steps 2~4,  $H^{m+1}(r)$  can be  
171 obtained.

172 3) The definition of the ApEn can be given as:

173 
$$ApEn(m, r) = \lim_{N \rightarrow \infty} [H^m(r) - H^{m+1}(r)] \quad (5)$$

174 If  $N$  is finite, formula 5 is rewritten as:

175 
$$ApEn(m, r, N) = H^m(r) - H^{(m+1)}(r) \quad (6)$$

176

## 177 **Multiscale approximate entropy**

178 To improve upon ApEn, the multiscale approximate entropy (MApEn) based on ApEn  
179 has been proposed to improve the robust and accuracy of model. Furthermore, the MApEn  
180 algorithm, overcomes the limitations of ApEn [17]. Interestingly, compared with only one  
181 feature obtained by ApEn, these MApEn values reflected by different scales are able to be used  
182 as a cluster of classification parameters for the subsequent SVM training model. The concrete  
183 steps of the MApEn algorithm are as follows [17]:

184 1) Assume the initial discrete series is  $X = \{x(i), i = 1, 2, \dots, N\}$ , and its length is  $N$ .

185 2) Construct a coarse time series  $\{z^{(\tau)}\}$ , where  $\tau$  represents the scale factor, and then, the  
186 scaling time series can be expressed as:

187 
$$z^\tau(j) = \frac{1}{\tau} \sum_{i=(j-1)\tau+1}^{j\tau} x(i) \quad 1 \leq j \leq N/\tau \quad (7)$$

188 Equation 7 is the same as the original sequence provided that the scale factor  $\tau=1$ .  
189 Furthermore, each coarse-graining series can be regarded as evenly dividing the original series,  
190 and each segmentation length is  $\tau$ .

191 By combining multiscales with the approximate entropy to generate MApEn, the MApEn  
192 algorithm is able to characterize the nonlinear information of series more effectively. Fig. 4  
193 exhibits the detailed flowchart.

194 **Fig. 4. Flowchart of Multiscale Approximate Entropy Algorithm.**

195

## 196 **MApEn algorithm and its performance**

197

### 198 **Fast ApEn algorithm and setting parameters**

199 First, we can calculate the ApEn according to the abovementioned equations 2~6. There  
200 is plenty of redundant computing in some steps; however, it is time-consuming and cannot be  
201 used for real-time determination. Bo et al. [18] proposed a type of fast ApEn algorithm that can  
202 shorten the running time by nearly 5 times. The main steps are as follows:

203 First step: The distance matrix  $D(N \times N)$  for the initial  $N$  points time sequence is  
204 calculated, and the element in the  $i^{th}$  row and  $j^{th}$  column can be denoted as  $d_{ij}$ . The rules for  
205 calculating  $d_{ij}$  are based on the following algorithm:

$$206 \quad d_{ij} = \begin{cases} 1 & |x(i) - x(j)| < r \\ 0 & |x(i) - x(j)| \geq r \end{cases} \quad i = 1 \sim N; j = 1 \sim N; i \neq j \quad (8)$$

207 Second step: assuming the dimension of the pattern vector  $m=2$ , we can easily obtain  
208 the values of  $C_i^2(r)$  and  $C_i^3(r)$  using equation 9.

209 
$$C_i^2(r) = \sum_{j=1}^{N-1} d_{ij} \cap d_{(i+1)(j+1)}$$

210 
$$C_i^3(r) = \sum_{j=1}^{N-2} d_{ij} \cap d_{(i+1)(j+1)} \cap d_{(i+2)(j+2)} \quad (9)$$

211 Third step: According to the values of  $C_i^2(r)$  and  $C_i^3(r)$ , then we get  $H_2(r)$  and  $H_3(r)$ .

212 Fourth step: The ApEn value can be calculated by equations 5~6.

213 Four parameters are involved in the MApEn algorithm: the length of the input signal  $N$ ,  
214 the dimension of the pattern vector  $m$ , the similar tolerance threshold value  $r$ , and the time  
215 scale factor  $\tau$ . For the ApEn algorithm, choosing the right parameters is of extreme importance  
216 to the algorithm.

217 After simulating several experiments, we finally select  $N = 1500, m = 2, r = 0.12 \times STD$  as  
218 our experimental parameters, where STD represents the standard deviation of initial time series.  
219 The ApEn values of the UWL signal of the two types of wheat at different tolerance thresholds  
220 were simulated using Matlab 2018a, and the results are shown in Fig. 5. As shown in Fig. 5, the  
221 ApEn values of the two types of wheat vary depending on different tolerance thresholds  $r$ .  
222 Although the ApEn values of the two types of wheat are small, the differences between the  
223 healthy and mouldy wheat are obvious based on the ApEn values, where  $r$  varies from 0.1 to  
224 0.19. In addition, another conclusion from the experimental results is that the smaller ApEn  
225 value of the mouldy wheat reflects that the activities of *Aspergillus* fungi are more regular and  
226 intensive than the healthy wheat itself, and thus, the value can be used as a classification feature  
227 to recognize mouldy wheat.

228 **Fig. 5. ApEn Values for Different Tolerance Thresholds of UWL Signals of Healthy and**  
229 **Mouldy Wheat.**

## 230 **Discussions**

231

### 232 **Performance analysis of the MApEn algorithm**

233 The ApEn algorithm only offers one classification feature; therefore, in order to  
234 overcome this shortcoming and get more classification feature values, the MApEn algorithm is  
235 introduced in this paper. For ApEn algorithm, the parameters  $N = 1500, m = 2, r = 0.12 \times STD$  are  
236 finally chosen and simulated via experiments. In addition to the parameters mentioned above, the  
237 scale factor  $\tau$  is a decisive factor in the performance of the MApEn algorithm. Due to the limited  
238 length of the initial time series,  $\tau$  is usually assigned a value from 2 to 10. The curve of the  
239 MApEn value at different scale factors is shown in Fig. 6.

#### 240 **Fig. 6. MApEn Values for Different Scale Factors of UWL Signals of Healthy and Mouldy** 241 **Wheat.**

242 Observing Fig. 6, the following conclusions can be achieved:

- 243 ① The MApEn values of the UWL of the two types wheat sample shows an inverse trend;
- 244 ② Compared with ApEn, the MApEn algorithm can offer several classification features that  
245 can be used at the same time under different scales rather than only one feature gained by  
246 ApEn algorithm.

247

### 248 **Bipartition classification and performance assessment by SVM**

249 To solve the classification problem between healthy and mouldy wheat, the SVM is  
250 introduced in this work. The SVM, proposed by Cortes and Vapnik [16] in 1995, is a type of  
251 linear classifier based on classification boundaries. Computationally, the striking points of the

252 SVM are how to choose the penalty and kernel parameters, and the kernel parameter impacts the  
253 nonlinear transformation of the input feature space from a lower-dimensional to a higher-  
254 dimensional space. In other words, this problem can be considered to be an optimization problem  
255 in which we seek to help the kernel function to find the optimal plane, by which we can conduct  
256 linearly separated classification based on a nonlinear transformation [19]. Although the training  
257 samples are not large enough, the SVM can achieve a good classification performance [20].  
258 Currently, the SVM has become one of most widely used learning algorithm, and it has been  
259 applied in various fields [21,22].

260         Based on the SVM method and the purpose of the classification, the three parameters in  
261 Table 1 and the ApEn value act as the classification features. The UWL signals of total groups of  
262 the two types wheat kernels have been trained, and then, the abovementioned 120 healthy and  
263 mouldy wheat samples are separately used as the testing group. Adopting the SVM training  
264 model offered by Lin's group from Taiwan University, the main parameters of the SVM are set  
265 as follows. The type of kernel function is a radial basis function, and the error value that  
266 terminates the iteration is 0.001. The ROC curve represents the classification result and is  
267 illustrated in Fig. 7, where the blue curve represents the classification performance of the  
268 MApEn algorithm, and the red curve represents the classification performance of the ApEn  
269 algorithm.

#### 270 **Fig. 7. The ROC Curves of Two Classification Models.**

271         From the ROC curves, Tables 2 and 3 can be calculated, where AUC, S.E., C.I., and PA  
272 represent the area under the curve, the standard error of the area, the confidence interval and the  
273 performance of the classifier, respectively. Comparing Table 2 with Table 3 shows that the  
274 classification accuracy rate based on MApEn has been improved obviously. In addition, the

275 standard error decreases by introducing the MApEn algorithm. The experimental results validate  
276 that the MApEn values can act as a cluster of main classification features to recognize wheat  
277 kernels as healthy or mouldy.

278 **Table 2. Classification Result Using ApEn as the Main Classification Feature.**

AUC	S.E.	95% C.I.	PA
0.8693	0.0272	[0.8260 0.9226]	Good

279 **Table 3. Classification Result Using MApEn as the Main Classification Features.**

AUC	S.E.	95% C.I.	PA
0.8874	0.0246	[0.8392 0.9356]	Good

280

## 281 **Conclusions**

282 The UWL signals from different conditions of wheat kernels can reflect their inner  
283 physiological and pathological changes; therefore, it can be used as an environmentally friendly  
284 and nondestructive method to assess wheat quality. Since the UWL signal is so sensitive to  
285 environmental factors and the inner states of wheat kernels, further studies and experiments  
286 seeking to minimize these influences caused by these factors need to be conducted.

287 Multiscale approximate entropy is introduced to analyse the UWL signals in this paper.  
288 Subsequently, we have used an SVM to establish the classification model. The results of the  
289 simulations via an experiment show that the MApEn algorithm is efficient and effective at  
290 analysing random UWL signals. One main deficiency is that we only establish a binomial  
291 classification model in this work due to the limited experimental data, and the MApEn algorithm  
292 fails to exhibit its advantages. Furthermore, recognizing mouldy wheat kernels is a continuous  
293 process during their storage period; therefore, establishing a multiclassification model to classify  
294 and recognize the degree of mould is of extreme significance to help the operators to acquire

295 accurate information about the degree of mould and make scientific choices, which requires  
296 further research to improve the precision of the established model.

297

## 298 **Acknowledgements**

299 The authors are grateful for all the reviewers and the editor for their valuable suggestions  
300 and comments.

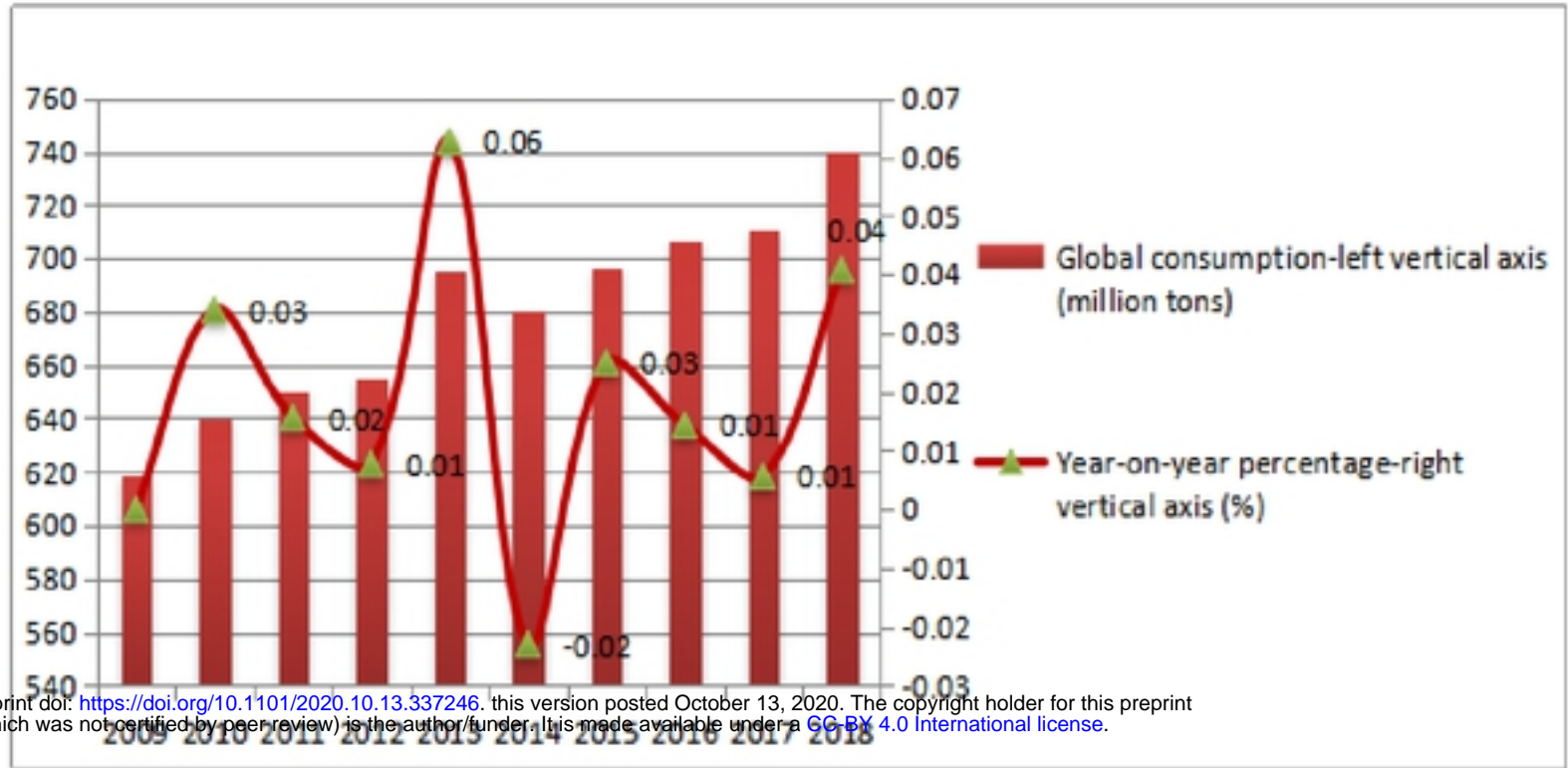
301

## 302 **References**

- 303 1. USDA. Grain: world markets and trade. United States: Department of Agriculture  
304 Foreign Agricultural Service; 2018.
- 305 2. CHYXX. 2019. Available from: <https://www.chyxx.com/industry/201910/793702.html>.
- 306 3. Milani J. Ecological conditions affecting mycotoxin production in cereals: a review. *Vet*  
307 *Med.* 2013;58: 405-411.
- 308 4. Heshmati A, Zohrevand T, Khaneghah AM, Nejad ASM, Sant'Ana AS. Co-occurrence of  
309 aflatoxins and ochratoxin A in dried fruits in iran: dietary exposure risk assessment. *Food*  
310 *Chem Toxicol.* 2017;106: 202-208.
- 311 5. Blankson G, Mill-Robertson F. Aflatoxin contamination and exposure in processed  
312 cereal-based complementary foods for infants and young children in greater Accra,  
313 Ghana. *Food Control.* 2016;64: 212-217.
- 314 6. Mhiko TA. Determination of the causes and the effects of storage conditions on the  
315 quality of silo stored wheat (*Triticum aestivum*) in Zimbabwe. *Nat Prod Bioprospecting.*  
316 2012;2: 21-28.
- 317 7. Gurwitsch A. Die natur des spezifischen erregers der zellteilung. *Arch Mikrosk Anat*  
318 *Entwicklungsmechanik.* 1923;100: 11-40.
- 319 8. Colli L, Facchini U, Guidotti G, Lonati RD, Orsenigo M, Sommariva O. Further  
320 measurements on the bioluminescence of the seedlings. *Experientia.* 1955;11: 479-481.
- 321 9. Popp FA, Gu Q, Li KH. Biophoton emission: experimental background and theoretical  
322 approaches. *Mod Phys Lett B.* 1994;8: 1269-1296.

- 323 10. Veselova T, Veselovsky V, Kozar V, Rubin A. Delayed luminescence of soybean seeds  
324 during swelling and accelerated ageing. *Seed Sci Technol.* 1988;16: 105-113.
- 325 11. Boschi F, Basso PR, Corridori I, Durando G, Sandri A, Segalla G, et al. Weak biophoton  
326 emission after laser surgery application in soft tissues: analysis of the optical features. *J*  
327 *Biophotonics.* 2019;12: e201800260.
- 328 12. Nirosha J, Murugan, Nicolas Rouleau, Lukasz M, Karbowski, Micheal A, et al.  
329 Biophotonic markers of malignancy: Discriminating cancers using wavelength-specific  
330 biophotons. *Biochemistry and Biophysics Reports.* 2018;13: 7-11.
- 331 13. Wang Z, Wang N, Li Z, Xiao F, Dai J. Human high intelligence is involved in spectral  
332 redshift of biophotonic activities in the brain. *Proc Natl Acad Sci U S A.* 2016;113: 8753-  
333 8758.
- 334 14. Duan S, Wang F, Zhang Y. Research on the biophoton emission of wheat kernels based  
335 on permutation entropy. *Optik.* 2019;178: 723-730.
- 336 15. Pincus SM. Approximate entropy as a measure of system complexity. *Proc Natl Acad Sci*  
337 *U S A.* 1991;88: 2297-2301.
- 338 16. Cortes C, Vapnik V. Support-vector networks. *Mach Learn.* 1995;20: 273-297.
- 339 17. Costa M, Goldberger AL, Peng CK. Multiscale entropy analysis of complex physiologic  
340 time series. *Phys Rev Lett.* 2002;89: 068102.
- 341 18. Bo H, Qingyu T, Fusheng Y, Tian-Xiang C. ApEn and cross-ApEn: property, fast  
342 algorithm and preliminary application to the study of EEG and cognition. *Signal Process.*  
343 1999;15: 100-108.
- 344 19. Chapelle O, Vapnik V, Bousquet O, Mukherjee S. Choosing multiple parameters for  
345 support vector machines. *Mach Learn.* 2002;46: 131-159.

- 346 20. Zhang Y, Wu L. Classification of fruits using computer vision and a multiclass support  
347 vector machine. *Sensors (Basel)*. 2012;12: 12489-12505.
- 348 21. Nagata F, Tokuno K, Mitarai K, Otsuka A, Ikeda T, Ochi H, et al. Defect detection  
349 method using deep convolutional neural network, support vector machine and template  
350 matching techniques. *Artif Life Robot*. 2019;24: 512-519.
- 351 22. Miyagi S, Sugiyama S, Kozawa K, Moritani S, Sakamoto SI, Sakai O. Classifying  
352 dysphagic swallowing sounds with support vector machines. *Healthcare (Basel)*. 2020;8:  
353 103.



bioRxiv preprint doi: <https://doi.org/10.1101/2020.10.13.337246>; this version posted October 13, 2020. The copyright holder for this preprint (which was not certified by peer review) is the author/funder. It is made available under a [CC-BY 4.0 International license](https://creativecommons.org/licenses/by/4.0/).

**Fig. 1**



bioRxiv preprint doi: <https://doi.org/10.1101/2020.10.13.337246>; this version posted October 13, 2020. The copyright holder for this preprint (which was not certified by peer review) is the author/funder. It is made available under a [CC-BY 4.0 International license](#).

**Fig. 2**

bioRxiv preprint doi: <https://doi.org/10.1101/2020.10.13.337246>; this version posted October 13, 2020. The copyright holder for this preprint (which was not certified by peer review) is the author/funder. It is made available under a [CC-BY 4.0 International license](#).

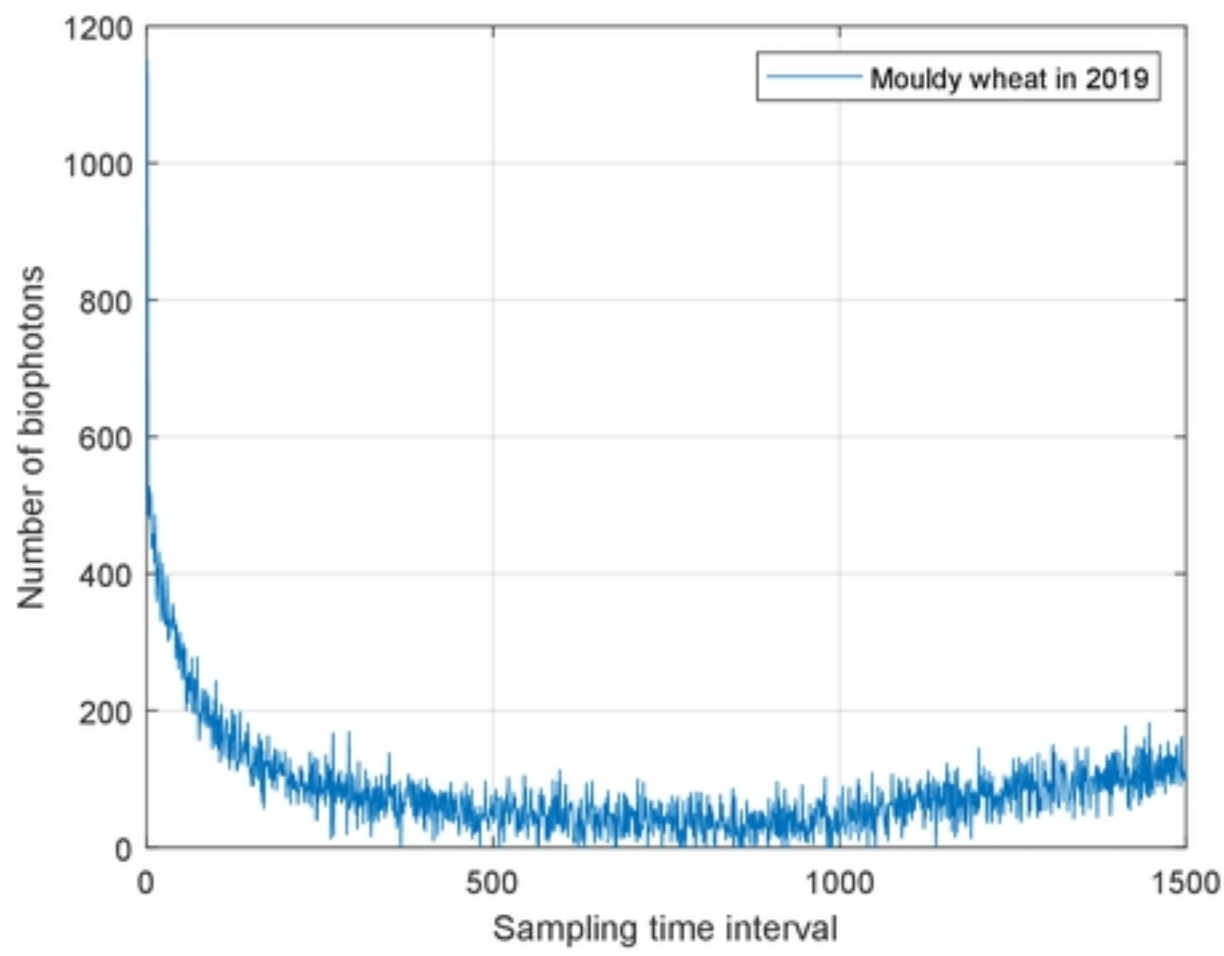
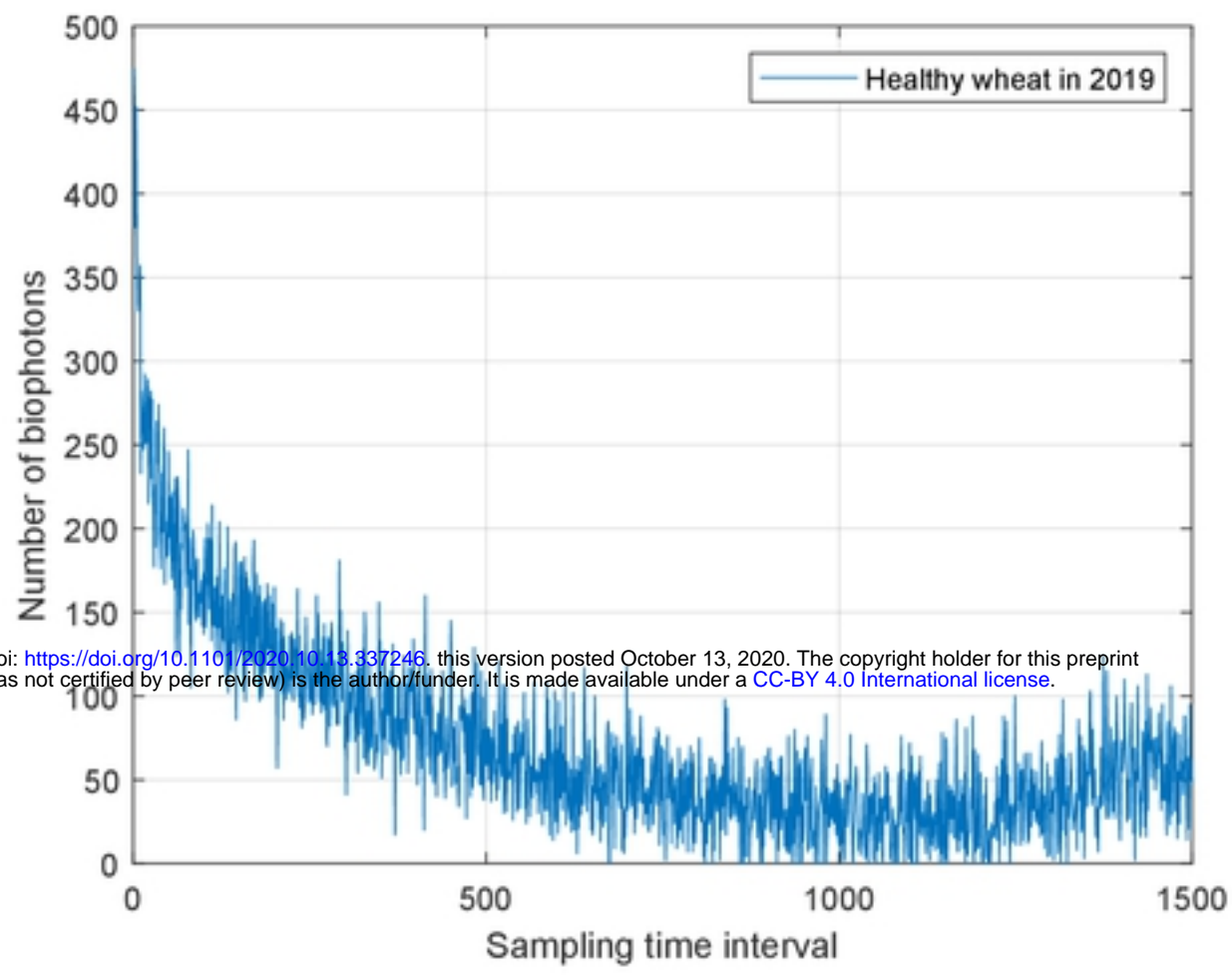


**Fig. 3**

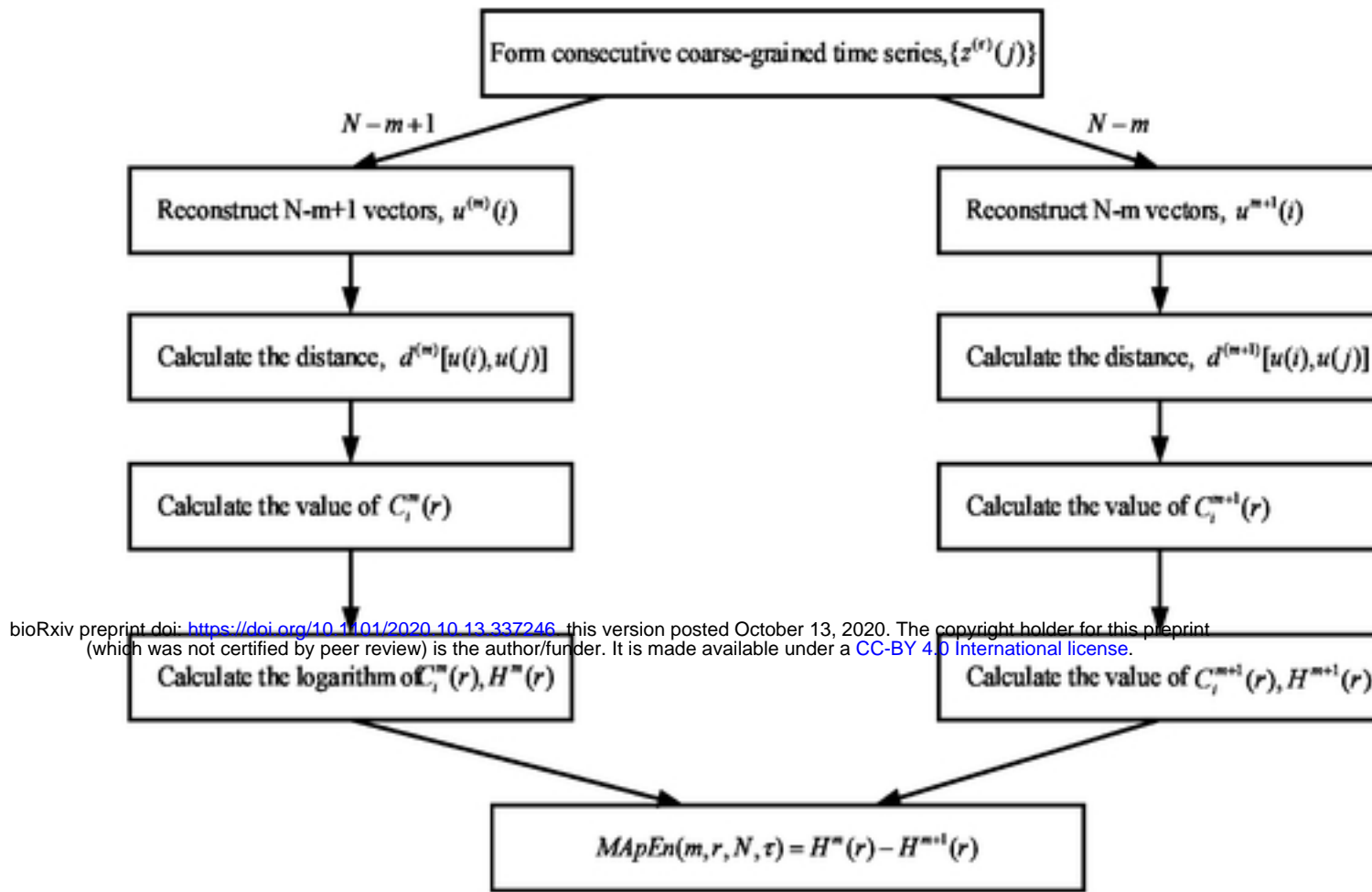


**Fig. 4**

bioRxiv preprint doi: <https://doi.org/10.1101/2020.10.13.337246>; this version posted October 13, 2020. The copyright holder for this preprint (which was not certified by peer review) is the author/funder. It is made available under a [CC-BY 4.0 International license](#).

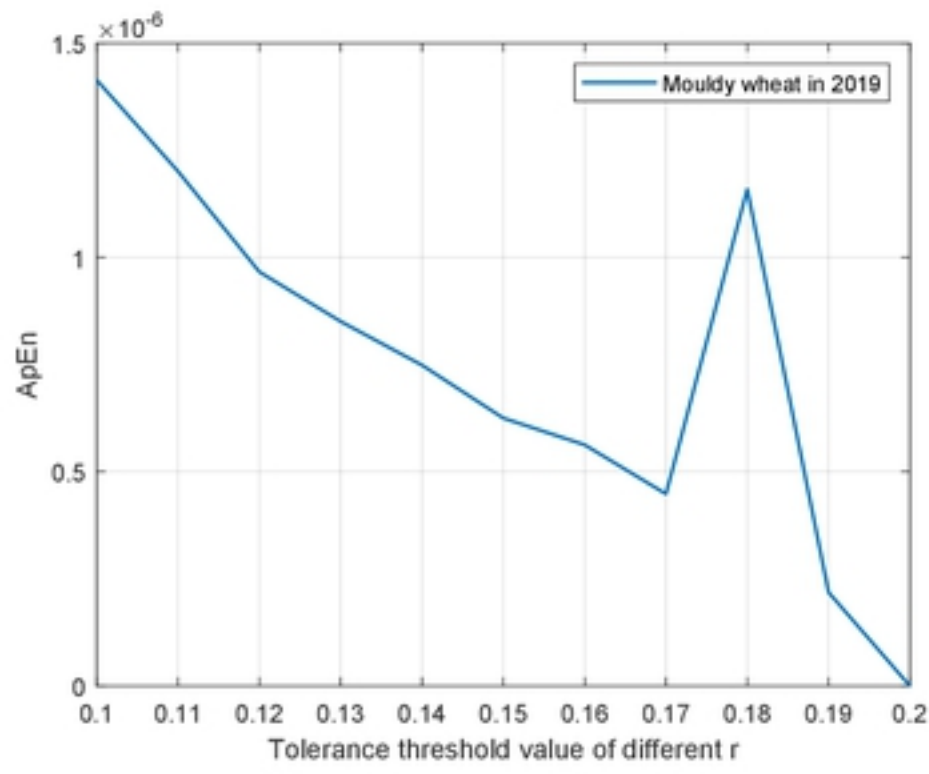
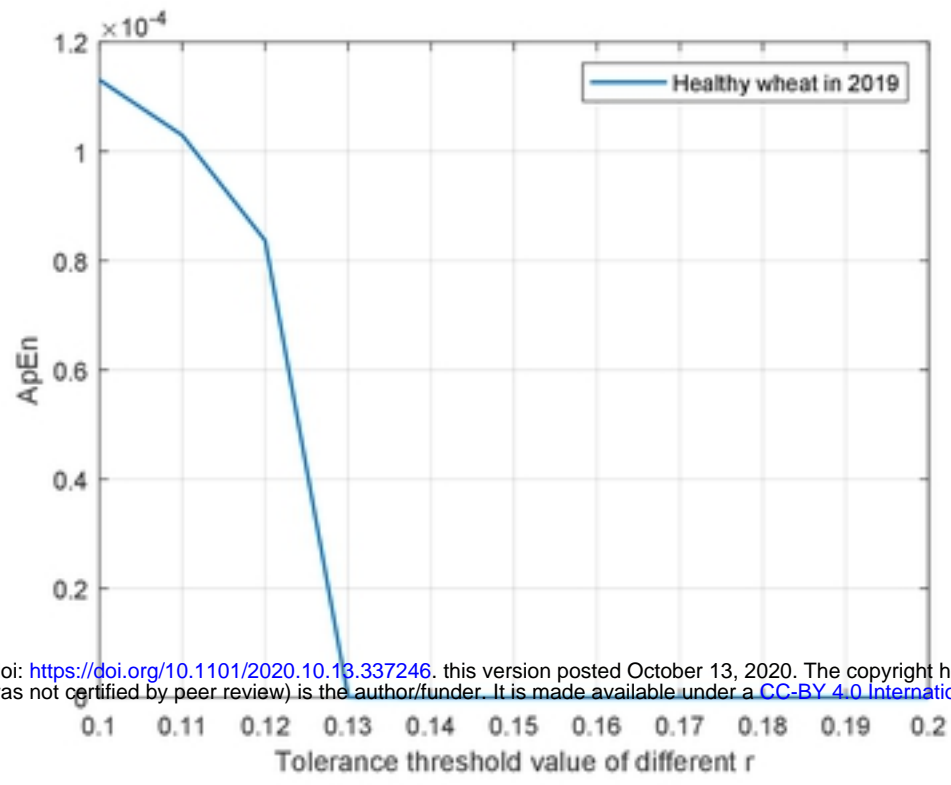
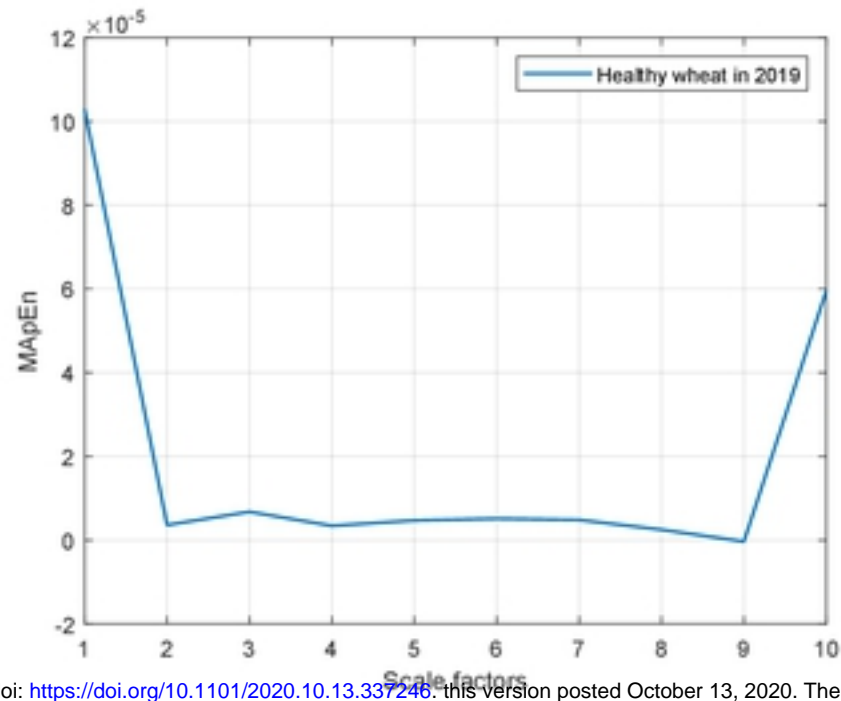


**Fig. 5**



bioRxiv preprint doi: <https://doi.org/10.1101/2020.10.13.337246>; this version posted October 13, 2020. The copyright holder for this preprint (which was not certified by peer review) is the author/funder. It is made available under a [CC-BY 4.0 International license](https://creativecommons.org/licenses/by/4.0/).

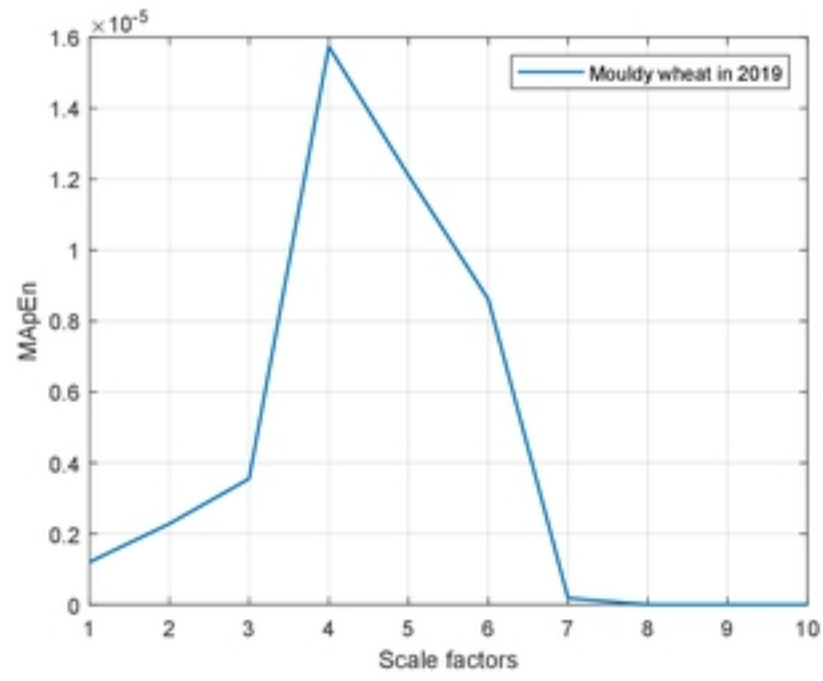
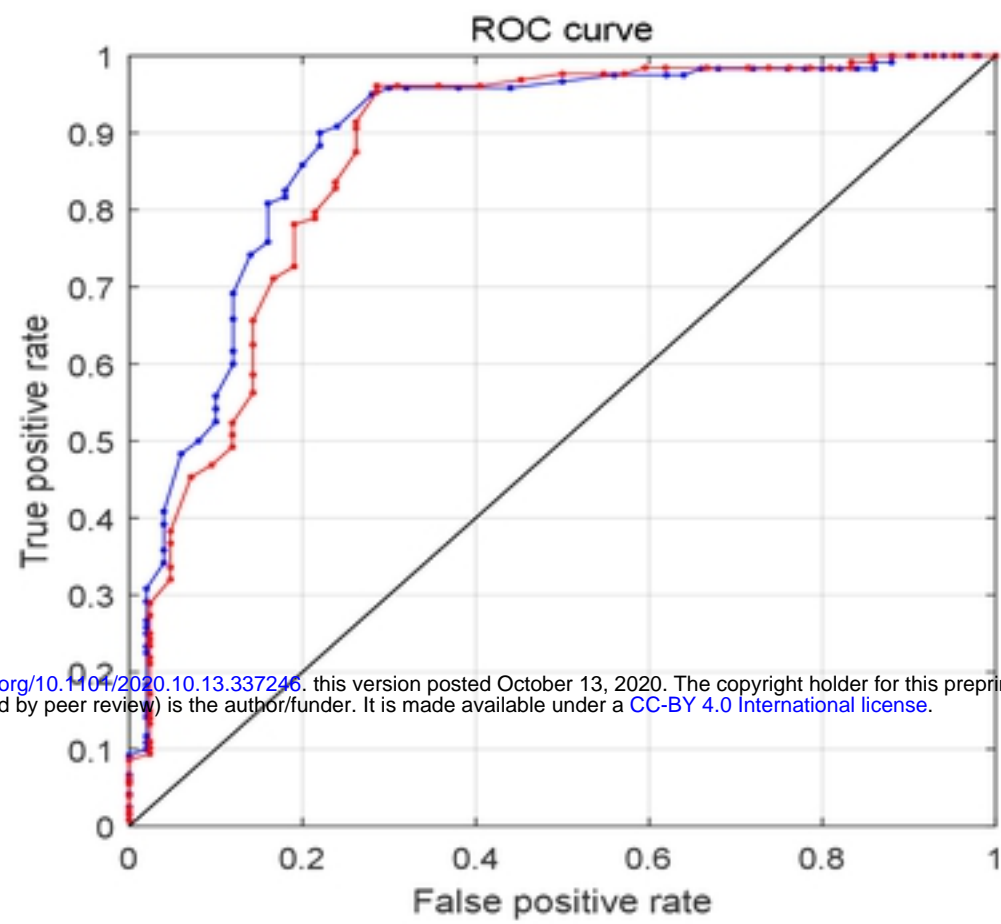


**Fig. 6**



bioRxiv preprint doi: <https://doi.org/10.1101/2020.10.13.337246>; this version posted October 13, 2020. The copyright holder for this preprint (which was not certified by peer review) is the author/funder. It is made available under a [CC-BY 4.0 International license](https://creativecommons.org/licenses/by/4.0/).

**Fig. 7**